A NEW HYBRID APPROACH TO DYNAMIC MODELING AND CONTROL DESIGN FOR A PECTORAL FIN PROPELLED UNMANNED UNDERWATER VEHICLE

Jason D. Geder[1] jgeder@lcp.nrl.navy.mil
John Palmisano[2] jpalmisano@cbmse.nrl.navy.mil
Ravi Ramamurti[1] ravi@lcp.nrl.navy.mil
William C. Sandberg[1] sandberg@lcp.nrl.navy.mil
Banahalli Ratna[2] bratna@cbmse.nrl.navy.mil

[1] **Laboratory for Computational Physics and Fluid Dynamics**
[2] **Center for Bio-molecular Science and Engineering**
Naval Research Laboratory, Washington, D.C. 20375

Abstract

A new hybrid approach to modeling and control design for a biologically inspired unmanned underwater vehicle using pectoral fin control force generation is presented in this paper. The full dynamics of the proposed vehicle are modeled and the forces produced by the fins are computed using computational fluid dynamics. The stability of motion in the dive plane is analyzed and a proportional-integral-derivative (PID) control system is designed. Geometric considerations are examined including fin placement, tail plane size and center of mass location. PID control of vehicle depth is implemented using fin surface curvature as a novel control variable. Using computer simulation, controlled vehicle motion is verified and desired maneuverability of the vehicle is achieved in the dive plane.

1. Introduction

Unmanned underwater vehicles (UUVs) have proven very useful in applications including inspection, surveillance, exploration and object detection. These applications are of extreme importance, especially in environments that are dangerous or impossible for a human to navigate. Current technology has allowed UUVs to excel at tasks including deep-sea diving, high-speed motion and long distance traversal. However, in the low-speed, high maneuverability operations required of many near-shore and littoral zone missions, UUV designs have found the environment challenging.

To confront the issue of low-speed maneuverability in the presence of ocean currents and near-shore obstacles, flapping fin mechanisms have been studied to understand how certain aquatic animals achieve their high levels of controllability. Colgate and Lynch (2004) have created a comprehensive summary of these studies. In one particular study, Blake (1979) determined that in low-speed operations labriform motion (using pectoral fin oscillation) is more efficient for maneuvering than carangiform motion (using body and caudal fin undulation). This result indicates that a flapping pectoral fin can be mounted on a rigid UUV hull without sacrificing low-speed maneuverability. Kato et al (2002) and Ando et al (2006) have developed both lift-based and drag-based deformable pectoral fins for use on UUVs. These fins, however, have not been shown to provide the precise controllability of surface curvature time-history that we have determined necessary to meet our hovering and low-speed maneuvering performance goals.

Walker and Westneat (1997) have studied the fin kinematics of a class of lift-based labriform fish, the bird wrasse (*gomphosus varius*), whose force production is a good match with our performance objectives. Ramamurti and Sandberg (2002) computationally studied the force production of the bird wrasse and achieved good agreement with Walker and Westneat (1997). This computational method used to study the bird wrasse has been applied to the design and development of an actively controlled-curvature biomimetic pectoral fin by Palmisano et al (2007).

A test vehicle is designed to demonstrate the force production capabilities of the mechanical pectoral fin built by Palmisano et al (2007). A complete six degree of freedom (6-DOF) dynamic model of the test vehicle is derived to simulate the dynamic response of the actual vehicle for use in control algorithm development. Because of the unique propulsion mechanism, assumptions that are traditionally made in UUV dynamics modeling must be rethought. The periodic vehicle oscillations caused by the flapping motion of the fins and the coupled thrust and lift forces are analyzed, and a control approach is employed that can accommodate these perturbations in steady swimming.

A control system is developed to dictate the motion of the vehicle in the vertical plane for initial onboard fin performance testing. This system utilizes control of the individual rib deflections on our biomimetic fin. Since no other actively controlled-curvature fin vehicle has been designed and built, the use of this additional degree of freedom to control a UUV is something that has never been explored.

2. Vehicle Design

A test vehicle is designed which will carry a set of two Naval Research Laboratory (NRL) actively controlled-curvature fins. This platform provides a means of demonstrating force production and controllability of the fins in an underwater test environment. Key hull design considerations include manufacturability, vertical plane stability, and drag reduction.

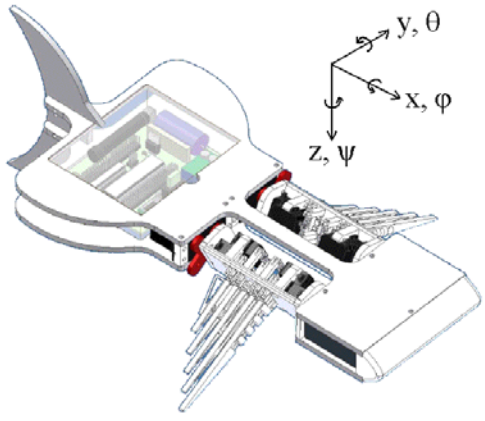

Fig. 1. Test vehicle showing fins, electronics and fixed vertical and horizontal tails.

The hull (Fig. 1) measures 1.3″ high, 13″ long and 7″ wide, and it has a dry weight of 2.2 pounds making it slightly negatively buoyant. The horizontal flat hull design is easy to manufacture, and also provides a high pitch moment of inertia improving stability in the vertical plane. To reduce vehicle drag and to better understand the flow field about the vehicle, CFD analysis was used during the design process (Fig. 2). It is also necessary to provide stabilizing surfaces including vertical and horizontal fixed tails to prevent yaw motion and further damp pitch oscillation.

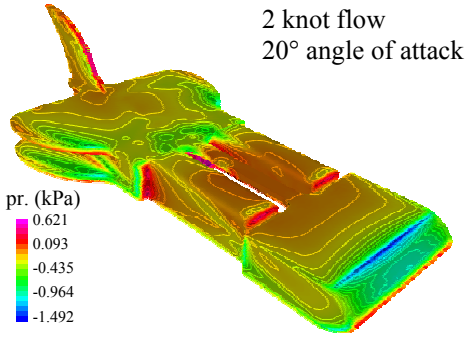

Fig. 2. Test vehicle CFD drag analysis.

A 3-axis accelerometer, 2 gyros, and a depth sensor are used to provide vehicle state feedback to an ATmega644 microcontroller. This microcontroller provides command output to both fins based on processed sensor data, and can be reprogrammed in-vitro as well as transmit real-time data wirelessly.

Given known fin power requirements (Palmisano et al 2007), a 2600mAh, 7V, NiMH battery will allow for 50 minutes of continuous full-speed runtime. Since the vehicle will spend much of its mission time in various modes at less than full-speed, battery life will be significantly longer.

3. Equations of Motion

Prior to completion of vehicle construction a dynamic model of the system is formulated to study performance and control system development. An undersea vehicle in motion consists of both rigid and elastic motions including control surface deflections and twisting of hydrodynamic surfaces. Specifically in the case of labriform motion produced by our biomimetic fins, there is significant elastic bending

and twisting. The rest of the body is assumed rigid, and as such, certain simplifications are made. The dynamics of a rigid body in 6-DOF motion are given in the following form (Fossen 1994):

$$\begin{aligned} &m\left(\left(\frac{\partial \vec{v}_0}{\partial t}\right)_r + \vec{\omega}\times\vec{v}_0 + \dot{\vec{\omega}}\times\vec{r}_G + \vec{\omega}\times\left(\vec{\omega}\times\vec{r}_G\right)\right) = \vec{f}_0 \\ &\tilde{I}_0\dot{\vec{\omega}} + \vec{\omega}\times\left(\tilde{I}_0\vec{\omega}\right) + m\vec{r}_G\times\left(\left(\frac{\partial \vec{v}_0}{\partial t}\right)_r + \vec{\omega}\times\vec{v}_0\right) = \vec{m}_0 \end{aligned} \tag{3.1}$$

where $\boldsymbol{v_0} = [u\ v\ w]^{\mathrm{T}}$, $\boldsymbol{\omega} = [p\ q\ r]^{\mathrm{T}}$, $\boldsymbol{r_G} = [x_G\ y_G\ z_G]^{\mathrm{T}}$, $\boldsymbol{I_0}$ is the inertia tensor at the origin of the body-fixed frame, $\boldsymbol{f_0} = [X\ Y\ Z]^{\mathrm{T}}$, and $\boldsymbol{m_0} = [K\ M\ N]^{\mathrm{T}}$. Substituting in this expanded notation yields the following equations:

$$\begin{aligned} &m[\dot{u} - vr + wq - x_G(q^2 + r^2) + y_G(pq - \dot{r}) + z_G(pr + \dot{q})] = X \\ &m[\dot{v} - wp + ur + x_G(qp + \dot{r}) - y_G(r^2 + p^2) + z_G(qr - \dot{p})] = Y \\ &m[\dot{w} - uq + vp + x_G(rp - \dot{q}) + y_G(qr + \dot{p}) - z_G(p^2 + q^2)] = Z \\ &I_x\dot{p} + (I_z - I_y)qr + I_{xy}(pr - \dot{q}) - I_{yz}(q^2 - r^2) - I_{xz}(pq + \dot{r}) \\ &\quad + m[y_G(\dot{w} - uq + vp) - z_G(\dot{v} - wp + ur)] = K \\ &I_y\dot{q} + (I_x - I_z)rp - I_{xy}(qr + \dot{p}) + I_{yz}(pq - \dot{r}) + I_{xz}(p^2 - r^2) \\ &\quad - m[x_G(\dot{w} - uq + vp) - z_G(\dot{u} - vr + wq)] = M \\ &I_z\dot{r} + (I_y - I_x)pq - I_{xy}(p^2 - q^2) - I_{yz}(pr + \dot{q}) + I_{xz}(qr - \dot{p}) \\ &\quad + m[x_G(\dot{v} - wp + ur) - y_G(\dot{u} - vr + wq)] = N \end{aligned} \tag{3.2}$$

Simplifications to this model can be made by placing the body-fixed coordinate frame at the center of buoyancy (*c.b.*). Also, we can assume symmetry about the *x-z* plane which yields $y_G = 0$, and $I_{xy} = I_{yz} = 0$. This reduces the rigid body equations to the following:

$$\begin{aligned} &m[\dot{u} - vr + wq - x_G(q^2 + r^2) + z_G(pr + \dot{q})] = X \\ &m[\dot{v} - wp + ur + x_G(qp + \dot{r}) + z_G(qr - \dot{p})] = Y \\ &m[\dot{w} - uq + vp + x_G(rp - \dot{q}) - z_G(p^2 + q^2)] = Z \\ &I_x\dot{p} + (I_z - I_y)qr - I_{xz}(pq + \dot{r}) - mz_G(\dot{v} - wp + ur) = K \\ &I_y\dot{q} + (I_x - I_z)rp + I_{xz}(p^2 - r^2) \\ &\quad - m[x_G(\dot{w} - uq + vp) - z_G(\dot{u} - vr + wq)] = M \\ &I_z\dot{r} + (I_y - I_x)pq + I_{xz}(qr - \dot{p}) + mx_G(\dot{v} - wp + ur) = N \end{aligned} \tag{3.3}$$

Condensing these equations into matrix form is desirable for manipulation of control parameters and design (Fossen 1994).

$$M\dot{\vec{v}} + C(\vec{v})\vec{v} + D(\vec{v})\vec{v} + \vec{g}(\vec{\eta}) = \vec{\tau} \tag{3.4}$$

where M is a matrix of rigid body mass and inertial terms, C is a matrix of centripetal and Coriolis terms, D is a matrix of hydrodynamic lift and drag terms, $\boldsymbol{g}$ is a vector of hydrostatic terms, $\boldsymbol{v} = [\boldsymbol{v_0}^{\mathrm{T}}\ \boldsymbol{\omega}^{\mathrm{T}}]^{\mathrm{T}}$, $\boldsymbol{\eta} = [x\ y\ z\ \phi\ \theta\ \psi]^{\mathrm{T}}$, and $\boldsymbol{\tau}$ is a vector of all forces and moments produced by the pectoral fins. In order to fill out these matrices we first need to determine the sources of all external forces and moments, $\boldsymbol{f_0}$ and $\boldsymbol{m_0}$.

4. Force and Moment Evaluation

The forces and moments acting on the vehicle can be represented by the sum of hydrodynamic, hydrostatic, and pectoral fin forces and moments. An exact solution of the hydrodynamic and pectoral fin terms requires solving the Navier-Stokes equations with boundary conditions. Unsteady computational fluid dynamic analysis is used to solve these equations to compute the instantaneous hydrodynamic forces and moments on the hull in response to external forces. Generally when coupled with 6-DOF equations of motion, a self-consistent vehicle trajectory computation using no coefficients is carried out, as is needed for novel underwater vehicle launch and recovery investigations (Ramamurti and Sandberg 2000).

For our control system design here we instead adopt a hybrid approach. Namely we use unsteady 3-D CFD to compute the force time-histories of the pectoral fins, since those are due to unsteady vorticity growth and shedding throughout the cycle, and incorporate those time-histories into our coefficient based equations for total body motion. We also explicitly incorporate added mass computations using Taylor series expansion and knowledge of simple geometric shapes into the inertial terms and CFD-based vehicle stability derivatives as our coefficients of the velocity terms.

4.1. Inertial Terms

Inertial forces produced by water that accelerates with the vehicle are included in the coefficient-based equations of motion as added mass terms. These terms can be expressed with coefficients defined by derivatives with respect to velocities and accelerations of the vehicle (Fossen 1994).

$$
\begin{aligned}
X_A &= X_{\dot{u}}\dot{u} + X_{wq}wq + X_{qq}q^2 + X_{vr}vr + X_{rr}r^2 \\
Y_A &= Y_{\dot{v}}\dot{v} + Y_{\dot{r}}\dot{r} + Y_{ur}ur + Y_{wp}wp + Y_{pq}pq \\
Z_A &= Z_{\dot{w}}\dot{w} + Z_{\dot{q}}\dot{q} + Z_{uq}uq + Z_{vp}vp + Z_{rp}rp \\
K_A &= K_{\dot{p}}\dot{p} + K_{vw}vw + K_{vq}vq + K_{wr}wr + K_{rq}rq \\
M_A &= M_{\dot{w}}\dot{w} + M_{\dot{q}}\dot{q} + M_{uw}uw + M_{uq}uq + M_{vp}vp + M_{rp}rp \\
N_A &= N_{\dot{v}}\dot{v} + N_{\dot{r}}\dot{r} + N_{uv}uv + N_{ur}ur + N_{wp}wp + N_{pq}pq
\end{aligned}
\tag{4.1}
$$

This notation is defined by eg. $X_{wq} = \partial^2 X/\partial w \partial q$. The values of all added mass coefficients derived from acceleration terms are computed in 4.2. The remaining cross-terms result from coupling and can be evaluated from the acceleration terms (Jakuba 2003, Ridley et al 2003).

For calculation of the added mass terms, the body is approximated as a rectangular prism. The prism is then divided into cross-sectional strips. Two-dimensional added mass terms are computed for each cross-section and then integrated over the third dimension (Patton 1965, Fossen 2004). This method of computing added mass is known as strip theory.

$$
\begin{aligned}
X_{\dot{u}} &= -\pi\rho a_{11}^2 \int_{-l/2}^{l/2} k_{11}(y,z)dx \\
Y_{\dot{v}_b} &= -\pi\rho a_{22}^2 \int_{-l/2}^{l/2} k_{22}(y,z)dx \\
Z_{\dot{w}} &= -\pi\rho a_{33}^2 \int_{-l/2}^{l/2} k_{33}(y,z)dx \\
K_{\dot{p}} &= -\pi\rho a_{33}^2 \int_{-w/2}^{w/2} y^2 k_{33}(x,z)dy - \pi\rho a_{22}^2 \int_{-h/2}^{h/2} z^2 k_{22}(x,y)dz \\
M_{\dot{q}} &= -\pi\rho a_{33}^2 \int_{-l/2}^{l/2} x^2 k_{33}(y,z)dx - \pi\rho a_{11}^2 \int_{-h/2}^{h/2} z^2 k_{11}(x,y)dz \\
N_{\dot{r}_b} &= -\pi\rho a_{11}^2 \int_{-w/2}^{w/2} y^2 k_{11}(x,z)dy - \pi\rho a_{22}^2 \int_{-l/2}^{l/2} x^2 k_{22}(y,z)dx \\
M_{\dot{w}} &= 0 \\
N_{\dot{v}} &= 0
\end{aligned}
\tag{4.2}
$$

where ρ is fluid density, k is a coefficient defined as a function of a/b, $2a$ is the dimension of the vehicle along the axis perpendicular to the direction of motion and $2b$ is the dimension along the axis parallel to the direction of motion. The limits of integration, l, w and h are the length, width and height of the vehicle, respectively.

The added mass due to the vertical tail plane must also be computed, and approximating the cross sectional area of the tail as a flat plate yields:

$$
Y_{\dot{v}_f} = \frac{1}{4}\pi\rho \int L_f(x)^2 dx, \qquad N_{\dot{r}_f} = \frac{1}{4}\pi\rho \int x^2 L_f(x)^2 dx \tag{4.3}
$$

where L_f is the span of the vertical tail plane.

4.2. Velocity Dependent Terms

Forces on the hull of the vehicle proportional to powers of the velocity can be resolved into body frame coordinates, denoted as lift, side force and drag. The moments can similarly be resolved into pitching, yawing and rolling moments. These forces and moments are characterized by the following relationships:

$$
\begin{aligned}
L &= \tfrac{1}{2}\rho C_L A_F V^2 & M_x &= \tfrac{1}{2}\rho C_{Mx} A_F V^2 \\
S &= \tfrac{1}{2}\rho C_S A_F V^2 & M_y &= \tfrac{1}{2}\rho C_{My} A_F V^2 \\
D &= \tfrac{1}{2}\rho C_D A_F V^2 & M_z &= \tfrac{1}{2}\rho C_{Mz} A_F V^2
\end{aligned}
\tag{4.4}
$$

where L is lift, S is side force, D is drag, M_x is moment about roll axis, M_y is moment about pitch axis, M_z is moment about yaw axis, A_F is the frontal area of the vehicle, V is the free stream velocity of the fluid and C_L, C_S, C_D, C_{Mx}, C_{My}, C_{Mz} are coefficients of lift, side force, drag, roll moment, pitch moment and yaw moment, respectively.

A 3-D model of the vehicle is created and inserted into a CFD simulation (Fig. 2). Running the simulation at various incoming flow speeds, angles of attack and sideslip angles allows us to create plots of the force coefficients. Each of these coefficients is a function solely of angle of attack (α) and sideslip angle (β). Lift is proportional to α, and side force is proportional to β. Drag is proportional to the squares of α and β. Moment is proportional to α in the pitch direction, and to β in the yaw direction. Improvements to vehicle geometry were made based on these computations to reduce drag. Plots of L vs. α, D vs. α, and M_y vs. α are given in Fig. 3. Plots of S vs. β, D vs. β, M_z vs. β are given in Fig. 4. From the information for lift, side force and drag we compute the hydrodynamic coefficients (Ridley et al 2003):

$$
\begin{aligned}
X_{u|u|} &= -\tfrac{1}{2}\rho A F(c_\alpha + c_\beta)/2 & X_{uw} &= -\tfrac{1}{2}\rho A_F b_\alpha \\
X_{uv} &= -\tfrac{1}{2}\rho A_F b_\beta & X_{ww} &= -\tfrac{1}{2}\rho A_F(a_\alpha + c_\alpha/2) \\
X_{v|v|} &= -\tfrac{1}{2}\rho A_F(a_\beta + c_\beta/2) & Y_{uvl} &= \tfrac{1}{2}\rho C_{S\beta} A_F \\
Y_{v|v|} &= \tfrac{1}{2}\rho A_F b_\beta & Y_{uvd} &= -\tfrac{1}{2}\rho A_F c_\beta \\
Z_{uwl} &= -\tfrac{1}{2}\rho C_{L\alpha} A_F & Z_{w|w|} &= -\tfrac{1}{2}\rho A_F b_\alpha \\
Z_{uwd} &= -\tfrac{1}{2}\rho A_F c_\alpha & M_{uwl} &= \tfrac{1}{2}\rho C_{My\alpha} A_F \\
N_{uvl} &= \tfrac{1}{2}\rho C_{Mz\beta} A_F
\end{aligned}
\tag{4.5}
$$

where a, b and c are defined by the quadratic fit to the C_D vs. α or β plots as $C_D = a_\alpha \alpha^2 + b_\alpha \alpha + c_\alpha$, or $C_D = a_\beta \beta^2 + b_\beta \beta + c_\beta$, respectively.

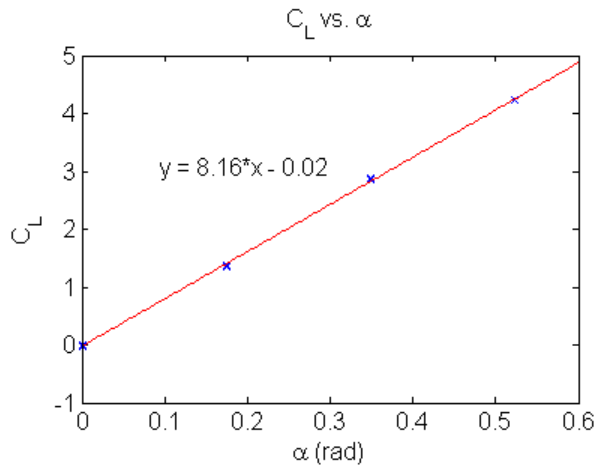

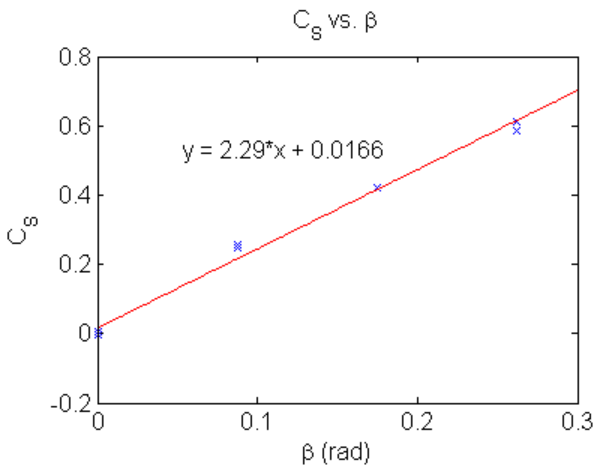

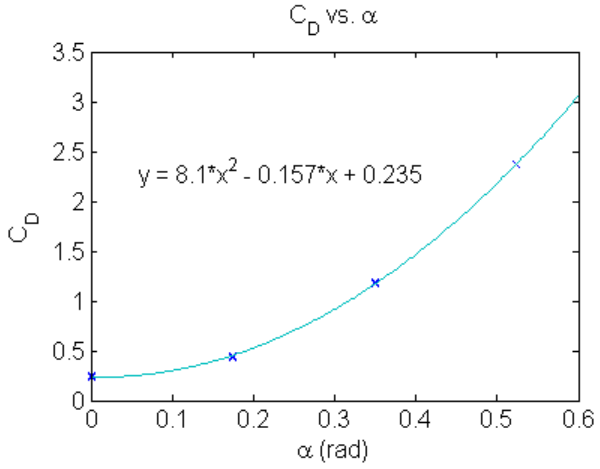

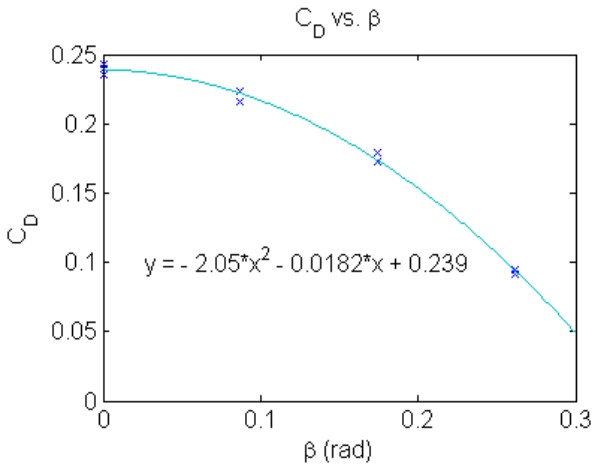

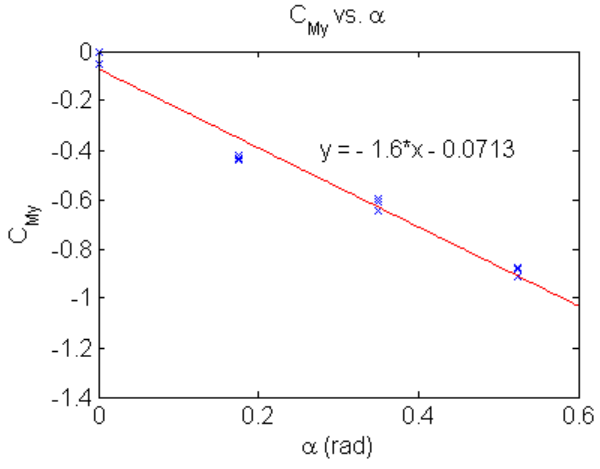

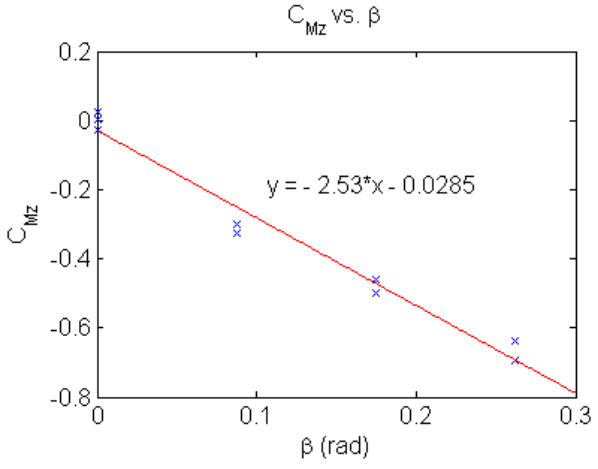

Fig. 3. C_L, C_D and C_{My} vs. α. β is set to zero.

Fig. 4. C_S, C_D and C_{Mz} vs. β. α is set to zero.

4.3. Hydrostatic Terms

Static forces and moments that act on the hull, weight (W) and buoyancy (B), depend on the orientation of the body and the location of the *c.g.* Simple geometry reveals that resolving the forces into the body-fixed frame yields the following equations:

$$
\begin{aligned}
X_{HS} &= -(W-B)\sin\theta \\
Y_{HS} &= (W-B)\cos\theta\sin\phi \\
Z_{HS} &= (W-B)\cos\theta\cos\phi \\
K_{HS} &= -y_G W\cos\theta\cos\phi - z_G W\cos\theta\sin\phi \\
M_{HS} &= -z_G W\sin\theta - x_G W\cos\theta\cos\phi \\
N_{HS} &= -y_G W\cos\theta\sin\phi - z_G W\sin\phi
\end{aligned} \tag{4.6}
$$

4.4. Pectoral Fin Force Time-Histories

The major difference in modeling the dynamics of a biomimetic underwater vehicle from a conventional underwater vehicle is in the propulsive mechanism. Traditionally, vehicles are driven by one or more ducted propellers oriented in such a way as to produce the desired thrust and lift vectors. In our model, a set of two robotic pectoral fins produces time varying thrust and lift given by the following equations.

$$
\begin{aligned}
X_{pec}(t) &= f_{lx}(t) + f_{rx}(t) \\
Y_{pec}(t) &= f_{ly}(t) - f_{ry}(t) \\
Z_{pec}(t) &= f_{lz}(t) + f_{rz}(t) \\
K_{pec}(t) &= -y_l f_{lz}(t) - y_r f_{rz}(t) \\
M_{pec}(t) &= x_l f_{lz}(t) + x_r f_{rz}(t) \\
N_{pec}(t) &= x_l f_{ly}(t) - x_r f_{ry}(t) - y_l f_{lx}(t) - y_r f_{rx}(t)
\end{aligned} \tag{4.7}
$$

The subscripts *l* and *r* denote the left and right fins respectively, and *x, y* and *z* indicate the body-frame direction in which the forces are produced by the fin.

In conventional propulsion the forces produced by each propeller are relatively easy to control and are generally aligned with one of the body frame axes so as to produce force along only one axis. In our pectoral fin approach to propulsion, the motion of the fin produces coupled time-varying forces in all three body axes. Furthermore, the control input to each fin cannot always be linearly mapped to a force. The control input instead directly yields the kinematics for the fin including a bulk rotation of the entire fin and a relative rotation for each of the ribs that comprise the fin. The implications of mapping an input signal to a fin force time-history for control of the vehicle are discussed in Section 6.

As detailed by Palmisano et al (2007), the variables that are modified directly include fin stroke amplitude, phase and frequency of bulk rotation, and individual rib deflection magnitudes. Fin angle of attack relative to the body is a fixed parameter for our design based upon the results of CFD optimization analysis (Ramamurti and Sandberg 2006).

4.5. Total External Forces

Combining force and moment terms for added mass, hull interaction, hydrostatic effect and pectoral fin motion (4.1, 4.5, 4.6, 4.7) and substituting into (3.3) yields:

$$
\begin{aligned}
&m[\dot{u} - vr + wq - x_G(q^2 + r^2) + z_G(pr + \dot{q})] = \\
&\quad X_{u|u|}u|u| + X_{\dot{u}}\dot{u} + X_{uv}u|v| + X_{uw}u|w| + X_{vv}v^2 + X_{vr}vr \\
&\quad + X_{ww}w^2 + X_{wq}wq + X_{qq}qq + X_{rr}rr - (W-B)\sin\theta + X_{pec} \\
&m[\dot{v} - wp + ur + x_G(qp + \dot{r}) + z_G(qr - \dot{p})] = \\
&\quad Y_{ur}ur + Y_{uv}uv + Y_{v|v|}v|v| + Y_{\dot{v}}\dot{v} + Y_{wp}wp \\
&\quad + Y_{pq}pq + Y_{\dot{r}}\dot{r} + (W-B)\cos\theta\sin\phi + Y_{pec} \\
&m[\dot{w} - uq + vp + x_G(rp - \dot{q}) - z_G(p^2 + q^2)] = \\
&\quad Z_{uw}uw + Z_{uq}uq + Z_{vp}vp + Z_{w|w|}w|w| + Z_{\dot{w}}\dot{w} \\
&\quad + Z_{\dot{q}}\dot{q} + Z_{rp}rp + (W-B)\cos\theta\cos\phi + Z_{pec} \\
&I_x\dot{p} + (I_z - I_y)qr - I_{xz}(pq + \dot{r}) - mz_G(\dot{v} - wp + ur) = \\
&\quad K_{\dot{p}}\dot{p} + K_{vw}vw + K_{vq}vq + K_{wr}wr \\
&\quad + K_{rq}rq - Wz_G\cos\theta\sin\phi + K_{pec} \\
&I_y\dot{q} + (I_x - I_z)rp + I_{xz}(p^2 - r^2) \\
&- mx_G(\dot{w} - uq + vp) + mz_G(\dot{u} - vr + wq) = \\
&\quad M_{uw}uw + M_{uq}uq + M_{vp}vp + M_{\dot{w}}\dot{w} + M_{\dot{q}}\dot{q} + M_{rp}rp \\
&\quad - Wz_G\sin\theta - Wx_G\cos\theta\cos\phi + M_{pec} \\
&I_z\dot{r} + (I_y - I_x)pq + I_{xz}(qr - \dot{p}) + mx_G(\dot{v} - wp + ur) = \\
&\quad N_{ur}ur + N_{uv}uv + N_{\dot{v}}\dot{v} + N_{wp}wp \\
&\quad + N_{pq}pq + N_{\dot{r}}\dot{r} - Wz_G\sin\phi + N_{pec}
\end{aligned} \tag{4.8}
$$

These are the 6-DOF hybrid equations of motion that fully describe the nonlinear dynamics of the test vehicle including the dynamics of the flapping motions of the NRL actively controlled-curvature fins.

5. Dive Plane Linearized Dynamics

To determine the thrust and lift performance of the NRL deforming fins, straight line motion of a vehicle is first considered. In this mode of motion, sway, yaw, and roll (*Y*, *N*, *K*) can be assumed zero leaving us with 3-DOF motion in the vertical plane characterized by surge, heave, and pitch (*X*, *Z*, *M*). This reduces the equations of motion to the following:

$$
\begin{aligned}
&m(\dot{u} + wq - x_G q^2 + z_G\dot{q}) = \\
&\quad X_{u|u|}u|u| + X_{\dot{u}}\dot{u} + X_{uw}u|w| + X_{ww}w^2 \\
&\quad + X_{wq}wq + X_{qq}qq - (W-B)\sin\theta + X_{pec}
\end{aligned} \tag{5.1}
$$

$$
\begin{aligned}
&m(\dot{w} - uq - x_G\dot{q} - z_G q^2) = \\
&\quad Z_{uw}uw + Z_{uq}uq + Z_{w|w|}w|w| + Z_{\dot{w}}\dot{w} \\
&\quad + Z_{\dot{q}}\dot{q} + (W - B)\cos\theta + Z_{pec} \\
&I_y\dot{q} - mx_G(\dot{w} - uq) + mz_G(\dot{u} + wq) = \\
&\quad M_{uw}uw + M_{uq}uq + M_{\dot{w}}\dot{w} + M_{\dot{q}}\dot{q} \\
&\quad - Wz_G\sin\theta - Wx_G\cos\theta + M_{pec}
\end{aligned}
\tag{5.1}
$$

It is desired to maintain a specific set of operating conditions to determine various vehicle motions. A linearized set of vehicle equations can be used to design a control algorithm for any steady, nominal condition. Further, this simplified control model allows our 8 MHz microcontroller to process feedback data in real-time.

Linearization about steady, level flight is considered in this paper, which is characterized by a nominal surge velocity and by zero values for heave and pitch velocities, and pitch angle. A linearization of (5.1) about this condition yields the following equations:

$$
\begin{aligned}
&m(\dot{u} + z_G\dot{q}) = \\
&\quad X_{u|u|}u_0|u| + X_{\dot{u}}\dot{u} + X_{uw}u_0|w| - (W - B)\theta + X_{pec} \\
&m(\dot{w} - u_0 q - x_G\dot{q}) = \\
&\quad Z_{uw}u_0 w + Z_{uq}u_0 q + Z_{\dot{w}}\dot{w} + Z_{\dot{q}}\dot{q} + (W - B) + Z_{pec} \\
&I_y\dot{q} - mx_G(\dot{w} - u_0 q) + mz_G\dot{u} = \\
&\quad M_{uw}u_0 w + M_{uq}u_0 q + M_{\dot{w}}\dot{w} + M_{\dot{q}}\dot{q} - Wz_G\theta - Wx_G + M_{pec}
\end{aligned}
\tag{5.2}
$$

This can be represented in matrix form simplified from (3.4) to allow implementation of classical control techniques. Similar linearizations can be made for any number of steady operating conditions. However, the example of steady, level flight is discussed here because it is the best operating mode to verify fin thrust production. After including linearized equations for θ, x and z, the following equation is setup:

$$
M\dot{\vec{x}} = F\vec{x} + G\vec{u} + \vec{H} \tag{5.3}
$$

Where $\boldsymbol{x} = [\boldsymbol{v}^T\ \boldsymbol{\eta}^T]^T$, $\boldsymbol{u} = [F_t^T\ F_l^T]^T$, F_t is the thrust produced by the fins and F_l is the lift produced by the fins. Provided that $\boldsymbol{M}$ is non-singular and adding an output equation we can write:

$$
\dot{\vec{x}} = A\vec{x} + B\vec{u} + \vec{E}, \qquad \vec{y} = C\vec{x} + D\vec{u} + \vec{F} \tag{5.4}
$$

Here $\boldsymbol{A}$ and $\boldsymbol{B}$ are the input state and control matrices, $\boldsymbol{C}$ and $\boldsymbol{D}$ are the output state and control matrices, and $\boldsymbol{E}$ and $\boldsymbol{F}$ are constant vectors.

6. Control Design

Unfortunately, running 3-D unsteady CFD force production computations for every possible set of fin kinematics is very time consuming. So instead of directly computing forces for all possible kinematics, trends must be observed over a range of operating conditions. Forces and moments for a few sets of fin kinematics are computed using CFD analysis, and force production for all other sets of kinematics are interpolated from the computed data to cover the entire control parameter space.

6.1. Control Parameters

It is possible to vary many of the parameters of the flapping kinematics which would affect the forces and moments produced by our fin. However, one parameter that we have chosen to remain constant is the fin root angle of attack. Allowing variability in angle of attack would necessitate additional hardware and mechanical complexity, and would also add unwanted weight to the vehicle. We have thus limited variability to parameters directly controllable by the servomotors for the bulk rotation of the fin and the individual deflections of each of the five ribs.

In evaluating controllability we started with predetermined nominal stroke amplitude, phase and individual rib deflection time-histories (Palmisano et al 2007). Using CFD analysis we have found that some fin parameters lend themselves to a wider range of performance variability than others. While achieving the desired maneuverability in 6-DOF will require control of a combination of these parameters, we will limit variability to a single parameter for initial testing in the vertical plane. This will allow us to accurately measure thrust and lift capabilities of the actively controlled curvature fin on the vehicle.

Varying stroke amplitude while keeping the other parameters fixed does not allow for much variability in lift, and indeed at a 2Hz flapping frequency only negative lift is generated by the fins over the range of useful amplitudes (Fig. 5). Varying fin stroke frequency allows for good thrust and lift variability, but is limited by maximum actuator response times.

We have found manipulating individual rib deflections is the best option for vertical plane

control using a single parameter. Maintaining a constant bulk rotation and flapping frequency for the stroke, varying individual rib deflection magnitude allows for a wide range of fin thrust and lift production (Fig. 7a). It is also the controllability of this parameter that makes our vehicle unique.

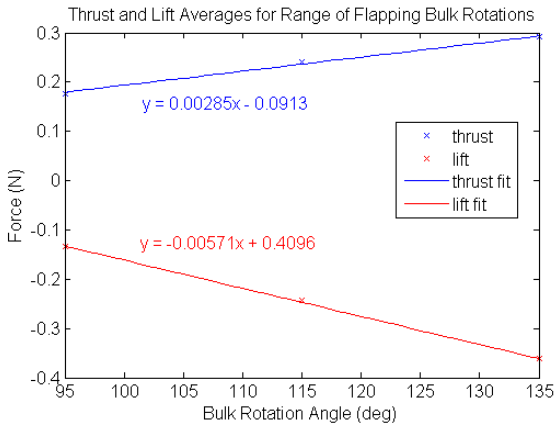

Fig. 5. Thrust and lift forces produced over range of operating amplitudes.

6.2. Open-Loop Behavior

We looked at simulated vehicle dynamic responses to the fins flapping at 2Hz and at the nominal stroke amplitude and phase (Palmisano et al 2007) over a range of individual rib deflections. Nonlinear responses to these fixed inputs show that the system is stable in heave and pitch without closed-loop control.

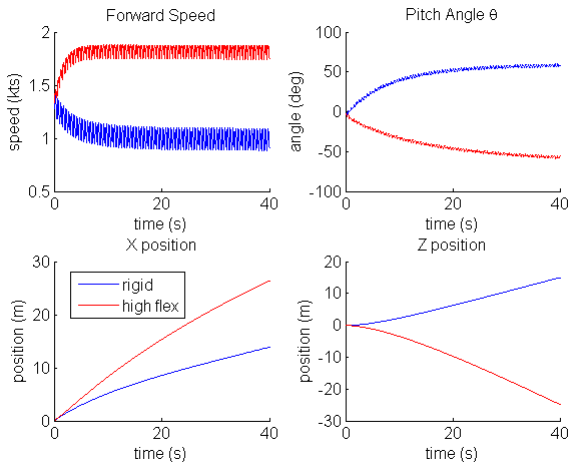

Fig. 6. Simulated open-loop responses of vehicle to fin flapping with rigid ribs (blue) and fully flexible ribs (red).

As Fig. 6 demonstrates, we see that while the open-loop responses are stable, the effect of individual rib deflection on the forward speed of the vehicle is dramatic. Fully flexible fins (red) provide enough thrust to yield a vehicle speed twice that of the vehicle speed with rigid fins (blue).

By modifying the fin surface curvature over time with specific kinematics sets, an entire range of lift and thrust vectors can be produced. To maintain a vehicle hover, the fins must produce kinematics that counters both the buoyancy imbalance and any external environmental disturbances.

6.3. Force and Moment Time-History Approximations

For any given set of fin kinematics the force time-histories are unique making it very difficult and time consuming to interpolate data to get a completely accurate force curve. For the purposes of simulation and control algorithm testing, we desire a more easily integrated method of approximating the forces produced by the fins. We found that the thrust and lift force averages plotted against a measure of individual rib deflection amplitude multiples can be accurately fitted with quadratic and linear functions, respectively (Fig. 7a). Similarly, the amplitudes of these force curves can be fitted with quadratic functions (Fig. 7b).

In order to assess whether these findings can be used in modeling the fin forces for our vehicle model, responses to static fin operating conditions were compared. Responses to a fully described CFD computed set of force time-histories were compared with responses to approximations of the same force time-histories using force averages with periodic sine functions (Fig. 8).

The results show very similar responses between the fully described time-history and the approximations. This is expected due to the relatively high flapping frequency compared to vehicle response time. The periodicity of the fin force curves (0.5s) is much smaller than can affect the general motion of the vehicle. This indicates that while CFD is necessary to optimize the actively deforming fin design and to compute the forces and moments produced by the fins at various flapping conditions, approximations of the time-histories using the force averages and amplitudes can be accurately implemented to model the vehicle system.

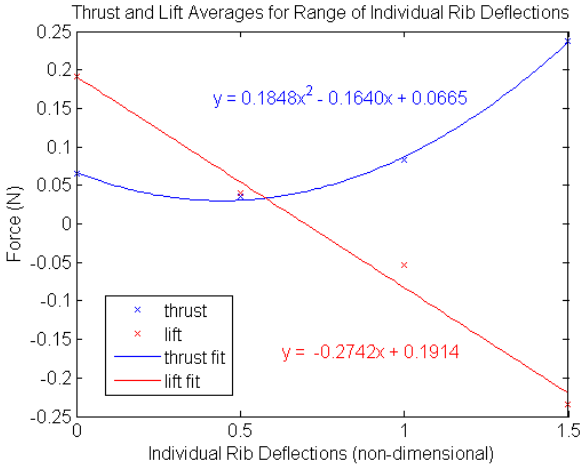

(a)

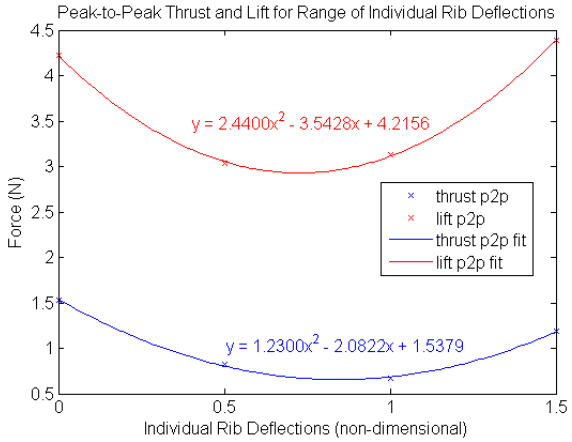

(b)

Fig. 7. Individual rib deflection effect on thrust and lift generation (a) average force curves (b) peak to peak force amplitude curves.

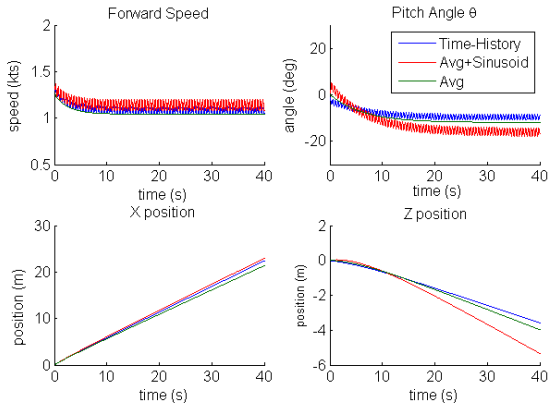

Fig. 8. Simulated open-loop responses to fin flapping with fully described force time-histories (blue), average force values plus sinusoidal variation (red), and average force values (green).

6.4. Control Method

The unique design and variable complexity of our propulsion mechanism and the low computational speed of the onboard microcontroller necessitate the use of non-conventional control techniques. For example, changing fin kinematics midstroke in response to updated sensor input could detrimentally affect vehicle performance. Since we have not yet fully studied the effects of adaptively changing the kinematics mid-stroke, only one kinematics set is used per stroke in all simulations.

A traditional control method for a dynamic model linearized about a selected mode of motion (i.e. steady, level flight) is to use a form of proportional-integral-derivative (PID) feedback control in conjunction with root locus and Bode analysis to measure stability. A PID controller for depth was designed and tested on a nonlinear vertical plane dynamic model of the vehicle simulation.

The presence of waves and currents that our vehicle will encounter necessitates the implementation of robust control techniques in which an unknown disturbance term is introduced to the system. For controlled laboratory testing of fin force production, however, these disturbances are negligible.

6.5. Frequency Domain and Stability Metrics

To use classical control techniques, the state-space representation of the vehicle dynamics is converted to frequency-space using Laplace transforms. Assuming we are interested in outputs of state variables, the matrices D and F from (5.4) are set to zero. Further assuming a time-invariant system, (5.4) is reformulated in the frequency-space as:

$$Y(s) = [C(sI - A)^{-1}B]U(s) + \frac{C(sI - A)^{-1}E}{s} \qquad (6.1)$$

Because the thrust fit equation (Fig. 7a) is a second order polynomial, we cannot account for it in our linear state space representation over a wide range of individual rib deflections. However, for control of depth this is relatively unimportant as the lift equation (Fig. 7b) has much more of an effect on depth. Assuming a loop feedback of the pitch rate (q), we can rewrite the transfer function from u to y as:

$$
\begin{aligned}
Y'(s) &= C(sI - A')^{-1} B'U'(s) + \frac{C(sI - A')^{-1} E'}{s} \\
A' &= A + 0.2742 K_q BC_q \\
B' &= -0.2742B \\
E' &= 0.1914B + E
\end{aligned} \tag{6.2}
$$

The feedback of pitch rate through a proportional gain (K_q) to the control of the vehicle is essential for damping the dynamic depth response which reduces overshoot and settling time.

Evaluating this model using root locus and Bode analysis is done using the discretized system with a sampling time of 1s. This time is an upper bound for the actual sampling time that will be used on the test vehicle, in order to ensure that the fins are flapping through complete cycles at a single operating condition.

Through simulation a K_q of 0.2 sufficiently damped the response while keeping the individual rib deflections within the limits of controllability. This yields the following discrete transfer function from *U'(z)* to *Y'(z)*:

$$
\frac{Y(z)}{U(z)} = \frac{-0.0595(z+1.153)(z-0.761)(z-0.536)(z+0.0119)}{(z-1)(z-0.768)(z-0.761)(z-0.368)(z-0.121)} \tag{6.3}
$$

Integral control will need to be used to eliminate any errors in depth caused by constant *E* matrix bias. An integral term will also be necessary in later vehicle trials when we deal with external disturbances such as ocean currents. The root locus and open-loop Bode plots of the discrete system using PI control are given in Fig. 9 which show the linear system to be stable.

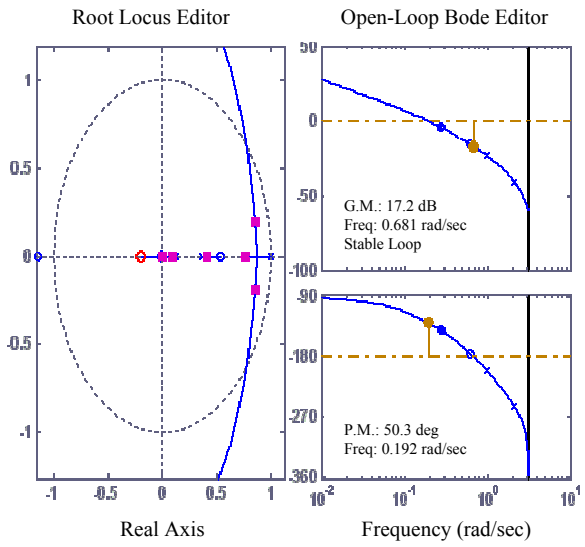

Fig. 9. Stability analysis of discrete linear vehicle system using root locus and bode plots

6.6. Closed-Loop Behavior

While the PID control algorithm is designed for a linear model, simulations implementing this control on the nonlinear 3-DOF vertical plane model are used to validate the design method. In Fig. 10, the nonlinear system (5.1) response is compared against the linearized system (5.2) response to a one meter depth change input. We see that the nonlinear and linear responses display very similar behavior including in depth overshoot and settling time. This lends support to the accuracy of using of the vehicle linearized model for both stability analysis and onboard vehicle control.

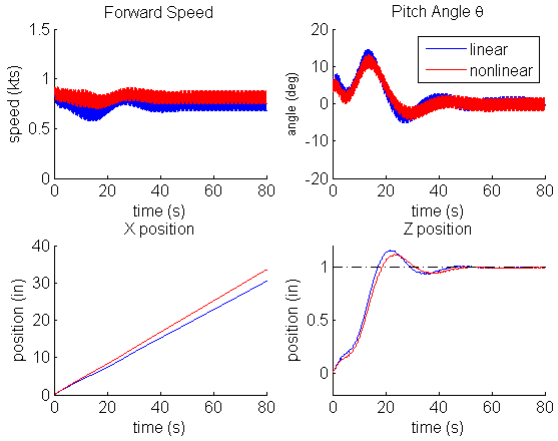

Fig. 10. Simulated vehicle response of linear (red) and nonlinear (blue) systems to one meter depth change command.

In using only one control variable (individual rib deflection) for this stage in vehicle testing, limiting flapping frequency based on mechanical constraints, we have successfully controlled vertical plane motion of the vehicle in simulation to demonstrate lift and thrust capabilities of the actively controlled-curvature pectoral fins designed and built by Palmisano et al (2007).

7. Future Work

The test vehicle is in the final stages of being manufactured and underwater tests will commence immediately upon completion. This will allow us to

verify the accuracy of the vehicle dynamic model presented in this paper.

Following initial testing for force production of the fins in a real underwater environment, more advanced control algorithm design will be implemented to account for the complex maneuvers desired of the 6-DOF nonlinear system. This will include allowing controllability of multiple fin parameters to achieve more independence between thrust and lift production, as well as improving control response time by allowing for parameter modification mid-stroke. We also plan for a full investigation into a wider range of fin kinematics to select for any desired vehicle thrust vector and magnitude.

Acknowledgment

All authors thank Dr. Kerr-Jia Liu for her work on the compliant rib design, her input at team meetings and her continued support of the project. All authors also thank Dr. James Kellogg of the Tactical Electronic Warfare Division at the Naval Research Laboratory for providing the high speed cameras needed to digitize the kinematics of the fin stroke.

References

Ando Y, Kato N, Suzuki H, Ariyoshi T, Suzumori K, Kanda T, Endo S, "Elastic Pectoral Fin Actuators for Biomimetic Underwater Vehicles", *Proceedings of the 16th International Offshore and Polar Engineering* Conference, 2006, pp. 260-267.

Blake RW, "The mechanics of labriform motion I. Labriform locomotion in the angelfish (*pterophyllum eimekei*): An analysis of the power stroke", *Journal of Experimental Biology*, vol. 82, 1979, pp. 255-271.

Colgate JE, Lynch KM, "Mechanics and Control of Swimming: A Review", *IEEE Journal of Oceanic Engineering*, vol. 29, pp. 660-673, Jul. 2004.

Fossen TI, *Guidance and Control of Ocean Vehicles*, John Wiley & Sons, New York, 1994.

Georgiades C, "Simulation and Control of an Underwater Hexapod Robot", Thesis, McGill University, 2005.

Jakuba M, "Modeling and Control of an Autonomous Underwater Vehicle with Combined Foil/Thruster Actuators", SM Thesis, WHOI-MIT Joint Program in Oceanographic Engineering, 2003.

Kato N, Liu H, Morikawa H, "Biology-Inspired Precision Maneuvering of Underwater Vehicles", *Proceedings of the 12th International Offshore and Polar Engineering* Conference, vol. 2, 2002, pp. 269-276.

Palmisano J, Ramamurti R, Lu K, Cohen J, Sandberg W, Ratna B, "Design of a Biomimetic Controlled-Curvature Robotic Pectoral Fin". *IEEE International Conference on Robotics and Automation*, Rome, IT, Apr. 2007.

Patton KT, "Tables of Hydrodynamic Mass Factors for Translational Motion", *ASME Paper No. 65-WA/Unt-2*, 1965.

Ramamurti R, Sandberg WC, "Computation of Two-Body Forces During UUV Retrieval", *Proceeding of the 1st International Symposium on Unmanned Undersea Vehicles*, Newport, RI, April 2000.

Ramamurti R, Sandberg WC, "Fluid dynamics of flapping aquatic flight in the bird wrasse: three-dimensional unsteady computations with fin deformation", *Journal of Experimental Biology*, vol. 205, 2002, pp. 2997-3008.

Ramamurti R, Sandberg WC, "Computational Fluid Dynamics Study for Optimization of a Fin Design", *Proceedings of the 24th AIAA Applied Aerodynamics Conference*, AIAA-2006-3658, 2006, San Francisco, CA.

Ridley P, Fontan J, Corke P, "Submarine Dynamic Modeling", *Australasian Conference on Robotics and Automation*, 2003.

Walker JA, Westneat MW, "Labriform Propulsion in Fishes: Kinematics of Flapping Aquatic Flight in the Bird Wrasse, *Gomphosus Varius* (Labridae)", *Journal of Experimental Biology*, vol. 200, 1997, pp. 1549-1569.